Journal of the Physical Society of Japan
Vol. 78, No. 4, April, 2009, 044710

Superconducting State of the Binary Boride Ru_7B_3 with the Noncentrosymmetric Crystal Structure

Naoki KASE and Jun AKIMITSU

Department of Physics and Mathematics, Aoyama Gakuin University, 5-10-1 Fuchinobe, Sagamihara, Kanagawa 229-8558

(Received November 12, 2008; accepted January 14, 2009; published April 10, 2009)

Single crystals of Ru_7B_3 were grown by the Czochralski puling method in a tetra-arc furnace. The compound crystallizes in a Th_7Fe_3-type structure (hexagonal, space group: $P6_3mc$), which has no inversion symmetry along the c-axis. Measurements in magnetic fields indicate type-II superconductivity with upper critical fields of $H_{c2}(0) \simeq 17.2$ kOe for $H \parallel [001]$ and 15.8 kOe for $H \parallel [100]$, respectively. The coherence length $\xi(0)_{GL}$, penetration depth $\lambda(0)_{GL}$, and Ginzburg–Landau (GL) parameter $\kappa(0)$ obtained from these values are 144 Å, 3110 Å, and 21.6 for $H \parallel [100]$, and 138 Å, 3520 Å, and 25.5 for $H \parallel [001]$, respectively. Specific heat measurements reveal that Ru_7B_3 is a weak-coupling superconductor with an isotropic superconducting gap.

KEYWORDS: Ru_7B_3, superconductivity, no inversion symmetry, specific heat
DOI: 10.1143/JPSJ.78.044710

1. Introduction

Since the discovery of a new heavy-fermion superconductor, $CePt_3Si$,[1] a noncentrosymmetric superconductor has been investigated to elucidate the novel superconducting pairing state in materials without inversion symmetry. Noncentrosymmetric heavy-fermion superconductors[1–4] show an unconventional behavior around the magnetic quantum critical point and exhibits coexisting superconductivity and magnetic ordering. This unusual state makes the materials more attractive, but that is the reason why the research field is too complicated to figure out the relationship between inversion symmetry breaking and superconductivity.

On the other hand, transition-metal compounds such as Li_2T_3B (T = Pd and Pt),[5,6] $Mg_{10}Ir_{19}B_{16}$,[7] and T_2Ga_9 (T = Rh and Ir)[8,9] are better candidates for examining the basic effects originating from a breaking inversion symmetry. The asymmetric spin–orbit coupling (ASOC) in noncentrosymmetric compounds leads to a breaking parity conservation and, therefore, the strength of the SOC, which is determined by the crystallographic structure, has a nontrivial effect on the symmetry of Cooper pairs. However, it is very difficult to synthesize the pure single crystals of these compounds owing to the difference in vapor pressure between the constituent elements. A single crystal is, therefore, highly desirable among non-centrosymmetric superconductors with no heavy-fermion nature.

T_7B_3 (T: transition metal) can be one of the potential systems for investigating the effect of non-centrosymmetry in a structure with 4d and 5d elements. The space group of T_7B_3 ($P6_3mc$) belongs to the non-centrosymmetric crystal symmetry. Ru_7B_3 was reported as a superconductor with $T_c = 2.58–3.38$ K using a polycrystalline sample,[10,11] despite the lack of report on its superconducting state.

To investigate the superconducting state more precisely, we have succeeded in growing single crystals of Ru_7B_3 using the Czochralski pulling method. This is a rare case for successfully making single crystals of a non-centrosymmetric superconductor in a non-heavy-fermion material. In this report, we reveal their superconducting and normal state properties on a pure single crystal of Ru_7B_3.

2. Experimental Details

Both polycrystals and single crystals were synthesized using a tetra-arc furnace. The polycrystal ingots were prepared by an arc-melting method with a fine Ru powder (99.9%) and an amorphous B powder (99.5%) with a nominal Ru/B ratio of 2.0, including an excess B powder in consideration of the low boron vapor pressure. The single crystals were grown by the Czochralski pulling method using the tetra-arc furnace in Ar atmosphere and growth rate was set to 10 mm/h. The single-crystalline nature was determined by the X-ray technique Laue method.

Both polycrystalline and single crystal samples were crushed into very fine powder and analyzed by the powder X-ray diffraction using a Cu Kα radiation to determine the crystal structure. Magnetic susceptibility and magnetization measurements were performed using a SQUID magnetometer (Quantum Design MPMSR2) in a temperature range of 1.8–4.0 K under various applied magnetic fields. Electrical resistivity was measured by a conventional DC four-probe method in a temperature range of 2.0–300 K under zero and various applied magnetic fields. The Specific heat measurements were performed with a PPMS system (Quantum Design) equipped with a ^{3}He refrigerator in a temperature range of 0.5–4.0 K under zero and various magnetic fields.

3. Results and Discussion

3.1 Crystal structure

The powder X-ray diffraction patterns for both polycrystalline and single crystal samples could be indexed as a Ru_7B_3 phase with the space group of $P6_3mc$. The lattice constants of the single crystal Ru_7B_3 were determined to be approximately $a = 7.441(5)$ Å and $c = 4.700(4)$ Å, respectively. The results are slightly narrower than those of polycrystalline sample ($T_c = 3.3$ K). The reported parameters of polycrystalline sample are $a = 7.467$ Å and $c = 4.713$ Å, respectively,[12] which are in good agreement with

Table I. Structural parameters for the Th_7Fe_3-type crystal structure.

Atom	Cite	x	y	z
Th1	2b	1/3	2/3	0.06
Th2	6c	0.126	0.874	0.250
Th3	6c	0.544	0.456	0.03
B	6c	0.815	0.185	0.31

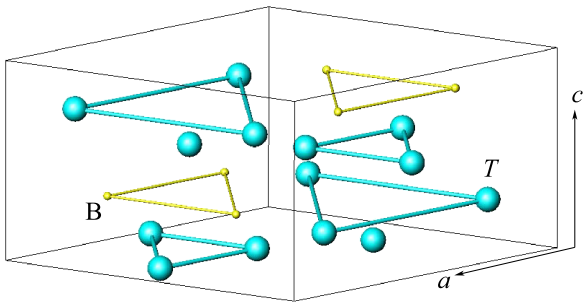

Fig. 1. (Color online) Crystal structure of Ru_7B_3 with a space group of $P6_3mc$. Large spheres correspond to Ru atoms and small ones to B atoms. The black lines show the hexagonal unit cell.

our polycrystalline sample. The structural parameters for the Th_7Fe_3-type are listed in Table I.[13)]

Ru_7B_3 crystallizes in a hexagonal structure with the space group of $P6_3mc$ (No. 186) as shown in Fig. 1. B atoms form triangles and these triangles are isolated from each other, because the positions of these triangles in a unit cell are not in the same plane. In addition, this crystal structure has no inversion symmetry along the c-axis. The space group symmetry of Ru_7B_3 belongs to the cyclic crystallographic class C_{6v} that has no inversion symmetry. Therefore, we can expect an unusual superconductivity due to the effect of Rashba-type ASOC in these compounds.

3.2 *Magnetic response*

The bulk nature of superconductivity in Ru_7B_3 was confirmed in the dc magnetic susceptibility $\chi(T)$ as shown in Fig. 2. The low-field susceptibility displays a strong diamagnetic signal due to a superconducting transition temperature with $T_c^{onset} = 2.8$ K. We confirmed that the polycrystalline sample shows $T_c^{onset} = 3.3$ K, being slightly higher than that of the single-crystal sample. What causes the difference in T_c might depend on the lack of Boron from the stoichiometry such as $Ln_2C_{3-\delta}$ (Ln = Y, La)[14–17)] or $NbB_{2-\delta}$.[18–22)] The fractional contraction of the lattice constants for the single crystals also supports the scenario.

Figure 3 shows the M–H curves of the sample at 1.9 K. The magnetization (M–H) curves indicate a typical type-II superconducting behavior. The lower critical field $H_{c1}(0)$ is defined as the field for deviating from the linear line for the initial slope. The lower critical field $H_{c1}(0)$ at zero temperature is discussed in §3.5.

3.3 *Electrical resistivity*

Figure 4 shows electrical resistivity as a function of temperature between 2.0 and 300 K. The onset and zero-resistivity temperatures were observed to be 2.95 and 2.8 K, respectively. Transition width can be defined as the temperature interval between 10 and 90% of the transition and

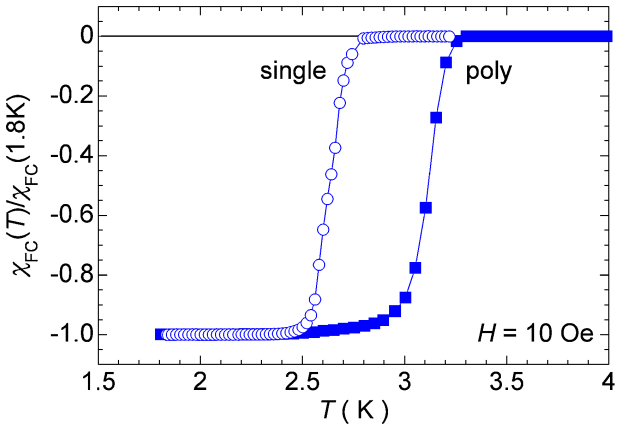

Fig. 2. (Color online) Temperature dependence of magnetic susceptibility $\chi(T)$ normalized by $\chi(T = 1.8\,\mathrm{K})$ under an applied magnetic field of 10 Oe for polycrystalline and single-crystal samples of Ru_7B_3.

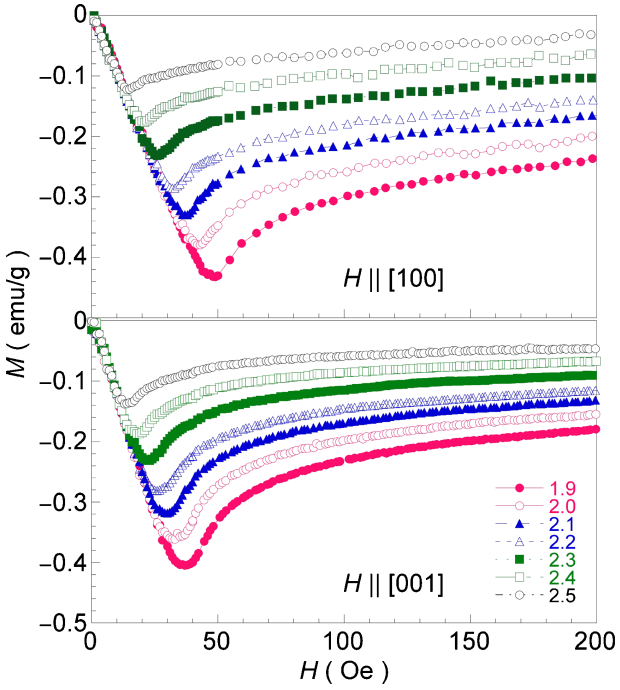

Fig. 3. (Color online) Magnetization curves vs magnetic fields $M(H)$ at several temperatures along [001] and [100].

is estimated to be approximately 0.1 K. The sharp superconducting transition indicates the high purity of the sample.

The electrical resistivity in the normal state decreases with decreasing temperature, showing a typical metallic behavior. The room-temperature resistivity $\rho(300\,\mathrm{K})$ is approximately 97 μΩ cm and the residual resistivity just above T_c, $\rho(\mathrm{res})$, is 26 μΩ cm for $J \parallel [100]$, and $\rho(300\,\mathrm{K}) = 55\,\mu\Omega\,\mathrm{cm}$, and $\rho(\mathrm{res}) = 14\,\mu\Omega\,\mathrm{cm}$ for $J \parallel [001]$. The residual resistivity ratio (RRR), therefore, is $\rho(300\,\mathrm{K})/\rho(\mathrm{res}) = 3.7$ for $J \parallel [100]$ and 3.9 for $J \parallel [001]$. Normal-state resistivity can be explained by a modified parallel resistor model.[23–27)] In this model, $\rho(T)$ is given by

$$\rho(T) = \left(\frac{1}{\rho_0 + \rho_{ph}} + \frac{1}{\rho_{max}}\right)^{-1}, \quad (1)$$

where ρ_0 is the residual resistivity, $\rho_{ph}(T)$ is the resistivity

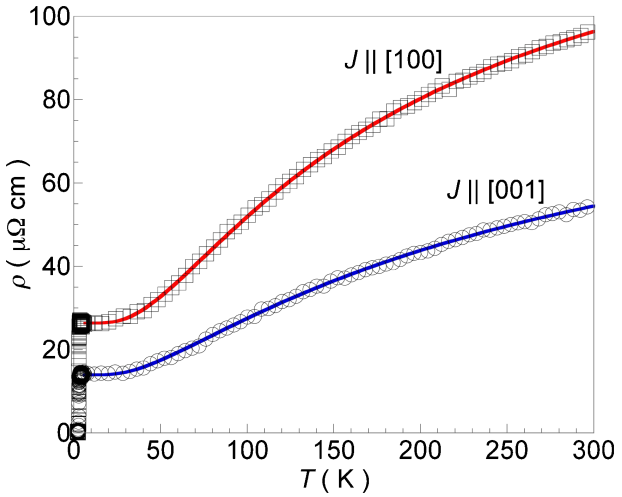

Fig. 4. (Color online) The temperature dependence of the electrical resistivity $\rho(T)$ of Ru_7B_3 between 2.0 and 300 K. The solid lines are the fitting results of eqs. (1) and (2). J represents current direction.

due to phonons, and ρ_{max} is the saturation resistivity, which is independent of temperature. Saturation resistivity is essentially the limiting resistivity when the electron mean free path l has become an interatomic spacing. The parameter $\rho_{ph}(T)$ is further given by

$$\rho_{ph}(T) = \alpha\left[\frac{E_1 - E_2}{k_B} + T\ln\left(\frac{e^{E_2/k_BT} - 1}{e^{E_1/k_BT} - 1}\right)\right], \qquad (2)$$

which can be derived by assuming that a thermal phonon with a flat energy distribution between E_1 and E_2 contributes to the scattering of conduction electrons and that the resistivity satisfies the Bose-Einstein statistics. Here, α and k_B are the fitting coefficient and Bolzmann's constant, respectively. Therefore, this formula allows us to estimate the energy distribution of the thermal phonon that gives rise to $\rho_{ph}(T)$. The experimentally obtained $\rho(T)$ values can be fitted with a curve using eqs. (1) and (2), and the fitting result is shown in Fig. 4. Using the fitting result, we estimate the phonon excitation energies of E_1 and E_2 to be 10 meV for $J \parallel [001]$, and 11–12 meV for $J \parallel [100]$, respectively. Therefore, thermal phonons with energies of 10 meV (∼120 K) for $J \parallel [001]$ and 11–12 meV (∼130–140 K) for $J \parallel [100]$, are much smaller than the Debye temperature $\Theta_D = 640$ K (see below). This result indicates that $\rho_{ph}(T)$ is predominantly contributed by a low-energy acoustic phonon.

3.4 *Specific heat*

The typical low-temperature specific heat in the temperature range between 0.4 and 4.0 K under several magnetic fields is presented in Fig. 5. In order to analyze the specific heat data, we use the expression $C(T) = \gamma_n T + \beta T^3$, where the first term is the electronic contribution ($= C_e$), γ_n is the electronic specific heat coefficient (Sommerfeld constant), and βT^3 ($= C_p$) is contributed by the lattice vibration. A standard analysis at 20 kOe yields a Sommerfeld constant $\gamma_n = 43.7$ mJ/(K^2 mol), and a Debye temperature $\Theta_D = 640$ K calculated from $\beta = N(12/5)\pi^4 R\Theta_D^{-3}$, where $R = 8.314$ J/(K mol), $N = 20$, and $\beta = 0.147$ mJ/(K^4 mol).

The bulk nature of superconductivity and good quality of the sample are confirmed by a sharp transition at $T_c = 2.8$ K,

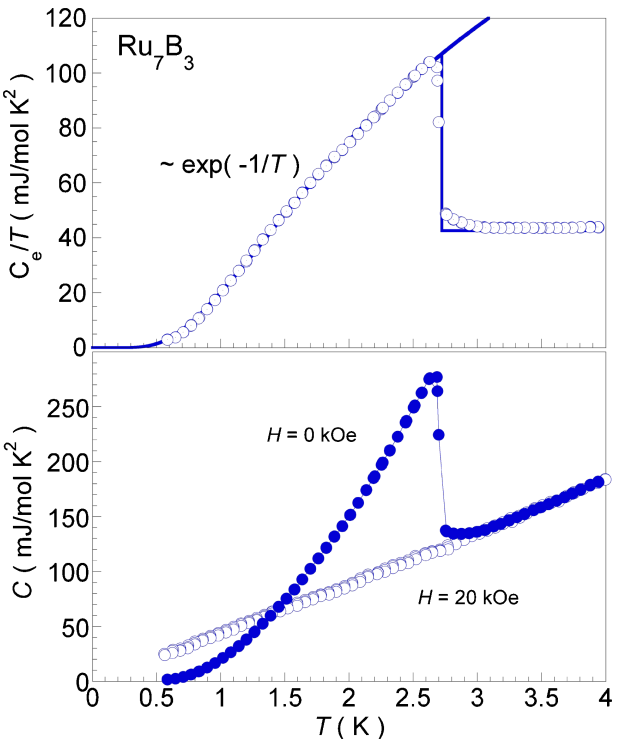

Fig. 5. (Color online) The upper panel shows the temperature dependence of the specific heat C_e/T of Ru_7B_3. The solid line represents C_e expected from the weak-coupling BCS theory. The down panel shows the temperature dependence of the specific heat C under 0 and 20 kOe.

which is in good agreement with T_c^{onset} determined by $\chi(T)$. The solid curve represents the fitting result obtained using the specific heat expression for a conventional superconductor ($C_e \sim \exp[-\Delta(0)/k_BT]$, where $\Delta(0)$ is the energy gap) below $0.8T_c$, where $\Delta(T)$ substantially deviates from $\Delta(0)$. Under a zero applied field, $C_e(T)$ shows an exponential temperature dependence at low temperatures. From the exponential dependence curve, the superconducting energy gap at a zero temperature $\Delta(0)$ can be estimated to be 0.38 meV. Using these values, we estimated $\Delta C_e/\gamma_n T_c$ to be approximately 1.4, which is almost identical to the value expected from the BCS weak-coupling limit ($\Delta C_e/\gamma_n T_c = 1.43$). Moreover, we calculated $2\Delta(0)/k_BT_c$ to be approximately 3.3, which is in rough agreement with the BCS value ($2\Delta(0)/k_BT_c = 3.52$).

The predominance of an s-wave channel is supported by the magnetic field dependence of the Sommerfeld parameter $\gamma(H)$, as shown in Fig. 6. The $\gamma(H)$ data was obtained from the specific heat C/T vs T^2 curve at 0.45 K under several magnetic fields (the inset of Figs. 6 and 7). For a highly anisotropic gap or a gap with nodes, the theory predicts a nonlinear $\gamma(H) \propto H^{1/2}$ dependence.[28] In contrast, for a fully gapped superconductor, $\gamma(H)$ should be proportional to the number of field-induced vortices, i.e., $\gamma(H) \propto H$. As shown in Fig. 6, the field-linear increase in $\gamma(H)$ suggests that most electronic states near the Fermi energy are fully gapped in Ru_7B_3.

3.5 *Upper and lower critical fields*

Figure 7 shows the temperature dependence of specific heat under various magnetic fields, to determine the upper critical field $H_{c2}(T)$. As shown Fig. 8, the $H_{c2}(T)$ shows

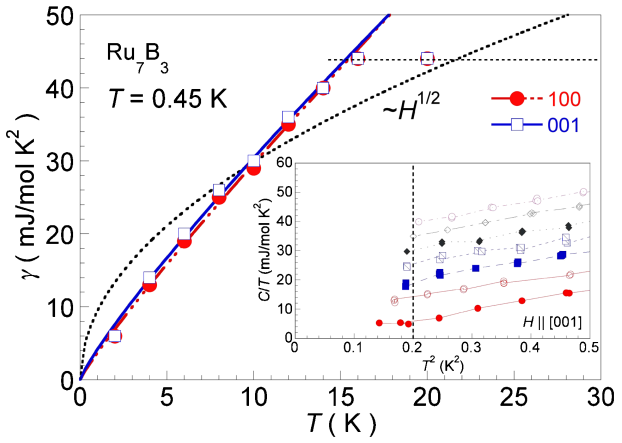

Fig. 6. (Color online) Magnetic field dependence of $\gamma(H)$ as a function of magnetic field at $T = 0.45$ K. The solid line corresponds to the linear relation ($\sim H$) and the dotted line represents the nonlinear relation ($\sim H^{1/2}$). The inset shows C/T vs T^2 under several magnetic fields (0–14 kOe) in the lowest-temperature region along $H \parallel [001]$.

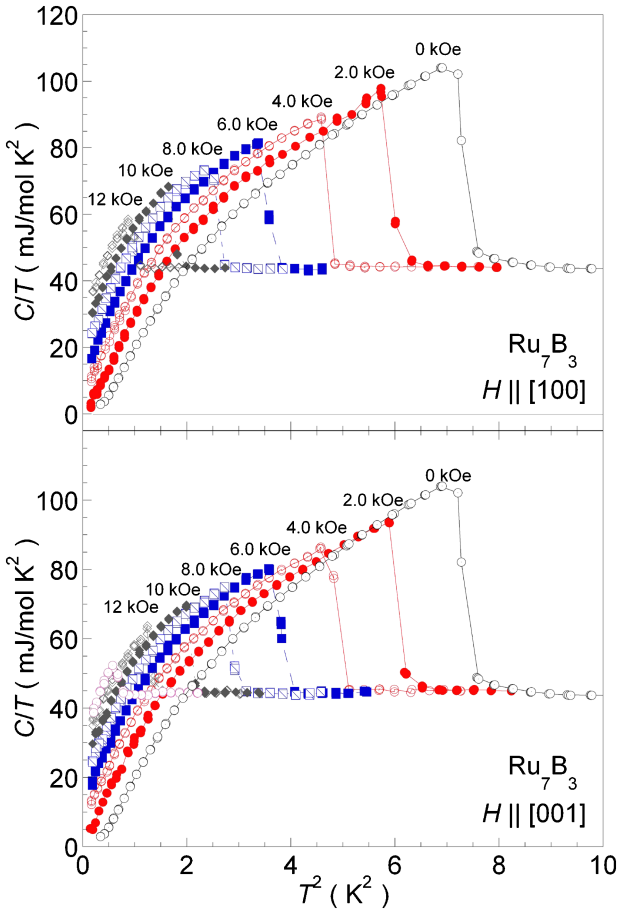

Fig. 7. (Color online) Temperature dependence of the specific heat C/T of Ru_7B_3 under several magnetic fields.

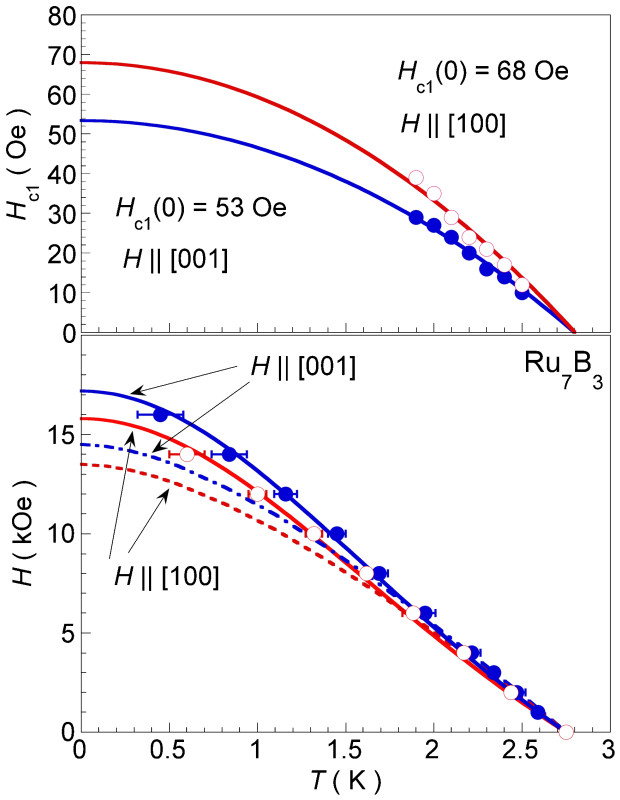

Fig. 8. (Color online) H_{c1} data are fitted to the formula $H_{c1}(T) = H_{c1}(0)[1 - (T/T_c)^2]$ (upper pannel). The lower panel shows the temperature dependence of the upper critical field H_{c2} for single-crystal Ru_7B_3. The solid line represents the fitting results obtained using GL theory and the dot line represents the WHH prediction.

an almost linear temperature dependence for the overall temperature region, which clearly deviates from the WHH prediction.[29,30] Because of the invalidity of using the WHH theory, we determined $H_{c2}(0)$ from the Ginzburg–Landau theory — $H_{c2}(T) = \phi_0/2\pi\xi^2(T)$, $\xi^2(T) = \alpha(T)(\hbar^2/2m^*)$, where ϕ_0 is the flux quantum, $\alpha(T) \propto (1 - t^2)/(1 + t^2)$, and $t = T/T_c$ is the reduced temperature; $H_{c2}(T)$ can be described as $H_{c2}(T) = [(1 - t^2)(1 + t^2)]H_{c2}(0)$. $H_{c2}(0)^{GL}$ was calculated to be approximately 17.2 kOe for $H \parallel [001]$ and 15.8 kOe for $H \parallel [100]$, respectively. Besides, the WHH theory predicted that the $H_{c2}(0)$ estimates will be approximately 15.2 kOe for $H \parallel [001]$ and 13.7 kOe for $H \parallel [100]$, respectively, following $H_{c2}(0) \simeq -0.693(dT/dT)_{T_c}T_c$. The slope dH_{c2}/dT was estimated to be -7.82 kOe/K for $H \parallel [001]$ and -7.07 kOe for $H \parallel [100]$ from the linear fitting result in the temperature range of $0.5 > T/T_c$.

The increased $H_{c2}(0)$ predicted from the WHH theory is estimated to be approximately 2.0 kOe for both [100] and [001]. The increase originated from the localization effects in highly disorder superconductors,[31] the anisotropy of the Fermi surface[32] and the strong electron–phonon coupling.[33,34] The present heat capacity measurements suggested that Ru_7B_3 belongs to a weak-coupling BCS superconductor with an isotopic s-wave pairing symmetry. It is inferred from these results that such a weak-coupling ratio and Fermi surface properties cannot be the source of H_{c2} increase. Another possibility is the localization effect. We have prepared a nonstoichiometric polycrystalline specimen, which is used in the present experiments as a sample with a nominal Ru/B ratio of 2.0 corresponding to excess boron. Thus, the localization effect induced by a deviation in stoichiometric Ru/B ratio also affects the temperature dependence of H_{c2} for Ru_7B_3 ($T_c \sim 2.8$ K), similarly to that of $H_{c2}(0)$ for $NbB_{2-\delta}$.[35]

The lower critical field $H_{c1}(0)$ is obtained from the M–H measurements at various temperatures. By using the conven-

Table II. Superconducting and normal state parameters for Ru_7B_3.

	[100]		[001]
Transition temperature, T_c (K)		2.8	
Thermodynamic critical field, $H_c(0)$ (Oe)	520		480
Critical field, $H_{c1}(0)$ (Oe)	68		53
Upper critical field, $H_{c2}(0)$ (kOe)	15.8		17.2
Penetration depth, $\lambda(0)$ (Å)	3110		3520
Coherence length, $\xi(0)$ (Å)	144		138
Ginzburg–Landauy parameter, $\kappa(0)$	21.6		25.5
T-linear coefficient, γ_n [mJ/(K^2 mol)]		43.7	
Debye temperature, $\Theta_D(K)$		640	
Superconducting energy gap, $\Delta(0)$ (meV)		0.38	
$\Delta C_e/\gamma_n T_c$		1.4	
$2\Delta(0)/k_B T_c$		3.3	

tional formula $H_{c1}(T) = H_{c1}(0)[1 - (T/T_c)^2]$, $H_{c1}(0)$ is estimated to be approximately 53 Oe for $H \parallel [001]$ and 68 Oe for $H \parallel [100]$.

We calculated the GL coherence length ξ_{GL} and magnetic penetration depth λ_{GL}, with the formulae $H_{c2} = \Phi_0/2\pi\xi_{GL}^2$, where Φ_0 is the flux quantum, and $H_{c1} = \Phi_0/\pi\lambda_{GL}^2$. The coherence length $\xi(0)_{GL}$ and the penetration depth $\lambda(0)_{GL}$ obtained using these formulae were estimated to be 144 and 3110 Å for $H \parallel [100]$, and 138 and 3520 Å for $H \parallel [001]$, respectively. By using the formula $\kappa(0) = \lambda(0)_{GL}/\xi(0)_{GL}$, the Ginzburg–Landau parameter $\kappa(0)$ was obtained to be 21.6 for $H \parallel [100]$ and 25.5 for $H \parallel [001]$, indicating that Ru_7B_3 is a type-II superconductor. The thermal critical field $H_c(0)$ was calculated to be 480 Oe for $H \parallel [001]$ and 520 Oe for $H \parallel [100]$, respectively, using the formula $H_c(0) = H_{c2}(0)/\sqrt{2}\kappa(0)$. Table II shows the measured and derived superconducting parameters.

4. Conclusions

Throughout all the experiments, we obtain no evidence of the noncentrosymmetric effect on superconducting properties. One of the reasons might be the weak electron correlation of the 4*d* electron of Ru. The anti-SOC effect of a 4*d* electron (Li_2Pd_3B) is much smaller than that of a 5*d* electron (Li_2Pt_3B). The energy splitting values of the bands at the Fermi surface are 200 meV (Li_2Pt_3B) and 20–50 meV (Li_2Pd_3B).[36] The result indicates that small-band splitting has no effect on the superconducting state. Thus, in the T_7B_3 system, Re_7B_3 has a possibility of exhibiting unconventional superconductivity, because it has a much stronger spin orbit interaction due to a 5*d* electron. The second reason is that the contribution of *d* electrons to the Fermi surface might be too small, such as that observed in T_2Ga_9 (T = Rh, Ir). In the Ga system, the contribution for the Fermi surface almost accounts for the *s*- or *p*-electrons of Ga-sites.[8] In the case of the T_7B_3 system, when a *d*-electron does not occupy a Fermi surface, the superconducting state is normal. To reveal a contribution of *d*-electron, an electrical calculation is strongly required.

The binary boride superconductor Re_7B_3 has a possibility of exhibiting unconventional superconductivity due to the much stronger spin orbit interaction of a 5*d* electron, when the contribution of a 5*d*-electron to the Fermi surface is significant. However, it is very difficult to synthesize a pure single crystal of Re_7B_3 because of the existence of many phases of the Re-B binary system. The single crystal growth of Re_7B_3 is currently in progress.

In conclusion, we reveal the physical properties in detail of the binary type-II superconductor, Ru_7B_3 by means of magnetic susceptibility $\chi(T)$, electrical resistivity $\rho(T)$, and magnetization $M(H)$ measurements. Ru_7B_3 crystallizes in a hexagonal structure with a space group of $P6_3mc$. Specific heat measurements indicated that Ru_7B_3 could be described by a conventional BCS superconductor in the weak-coupling regime. On the basis of the temperature dependence of C_{el} below T_c, we conclude that the symmetry of superconductivity of Ru_7B_3 corresponds to an isotropic *s*-wave symmetry.

Acknowledgments

This work was partially supported by the "High-Tech Research Center Project" for Private Universities and a Grand-in-Aid for Scientific Reaserch on Priority Area (No. 16076212) from the Ministry of Education, Culture, Sports, Science and Technology. One of the authors (N. Kase) acknowledges the support of the "Iwanami Fujukai Foundation".

1) E. Bauer, G. Hilscher, H. Michor, Ch. Paul, E. W. Scheidt, A. Gribanov, Yu. Seropegin, H. Noel, M. Sigrist, and P. Rogl: Phys. Rev. Lett. **92** (2004) 027003.
2) T. Akazawa, H. Hidaka, T. Fujiwara, T. C. Kobayashi, E. Yamamoto, Y. Haga, R. Settai, and Y. Ōnuki: J. Phys.: Condens. Matter **16** (2004) L29.
3) N. Kimura, K. Ito, K. Saitoh, Y. Umeda, H. Aoki, and T. Terashima: Phys. Rev. Lett. **95** (2005) 247004.
4) I. Sugitani, Y. Okuda, H. Shishido, T. Yamada, A. Thamizhavel, E. Yamamoto, T. D. Matsuda, Y. Haga, T. Takeuchi, R. Settai, and Y. Ōnuki: J. Phys. Soc. Jpn. **75** (2006) 043703.
5) K. Togano, P. Badica, Y. Nakamori, S. Orimo, H. Takeya, and K. Hirata: Phys. Rev. Lett. **93** (2004) 247004.
6) P. Badica, T. Kondo, and K. Togano: J. Phys. Soc. Jpn. **74** (2005) 1014.
7) T. Klimczuk, Q. Xu, E. Morosan, J. D. Thompson, H. W. Zandbergen, and R. J. Cava: Phys. Rev. B **74** (2006) 220502R.
8) T. Shibayama, M. Nohara, H. Aruga-Katori, Y. Okamoto, Z. Hiroi, and H. Takagi: J. Phys. Soc. Jpn. **76** (2007) 073708.
9) K. Wakui, S. Akutagawa, N. Kase, K. Kawashima, T. Muranaka, F. Iwahori, J. Abe, and J. Akimitsu: J. Phys. Soc. Jpn. **78** (2009) 034710.
10) B. T. Matthias, V. B. Compton, and E. Corenzwit: J. Phys. Chem. Solids **19** (1961) 130.
11) J. M. Vandenberg, B. T. Matthias, E. Corenzwit, and H. Barz: Mater. Res. Bull. **10** (1975) 889.
12) B. Anderson: Acta Chem. Scand. **13** (1959) 109.
13) J. V. Florio, N. C. Baenziger, R. E. Runble: Acta Crystallogr. **9** (1956) 367.
14) A. Simon and Th. Gulden: Z. Anorg. Allg. Chem. **630** (2004) 2191.
15) J. S. Kim, W.-H. Xie, R. K. Kremer, V. Babizhetskyy, O. Jepsen, and A. Simon: Phys. Rev. B **76** (2007) 014516.
16) M. C. Krupka, A. L. Giorgi, N. H. Krikorian, and E. G. Szklarz: J. Less Common Met. **17** (1969) 91.
17) G. Amano, S. Akutagawa, T. Muranaka, Y. Zenitani, and J. Akimitsu: J. Phys. Soc. Jpn. **73** (2004) 530.
18) A. S. Cooper, E. Corenzwit, L. D. Inginotti, B. T. Matthias, and W. H. Zachariasen: Proc. Natl. Acad. Sci. U.S.A. **67** (1970) 313.
19) L. Leyarovska and E. Layarovski: J. Less Common Met. **67** (1979) 249.
20) J. E. Schirber, D. L. Overmyer, B. Morosin, E. L. Venturini, R. Baughman, D. Emin, H. Klensnar, and T. Sdelage: Phys. Rev. B **45** (1992) 10787.
21) A. Yamamoto, C. Takao, T. Masui, M. Izumi, and S. Tajima: Physica C **383** (2002) 197.

22) R. Escamilla, O. Lovera, T. Akachi, A. Durán, R. Falconi, F. Morales, and R. Escudero: J. Phys.: Condens. Matter **16** (2004) 5979.
23) S. Ramakrishnan, K. Ghosh, A. D. Chinchure, V. R. Marathe, and G. Chandra: Phys. Rev. B **52** (1995) 6784.
24) H. Wiesmann, M. Gurvitch, H. Lutz, A. Ghosh, B. Schwarz, M. Strongin, P. B. Allen, and J. W. Halley: Phys. Rev. Lett. **38** (1977) 782.
25) E. S. Hellman and E. H. Hartford, Jr.: Phys. Rev. B **47** (1993) 11346.
26) M. Kasahi, S. Abe, T. Taniguchi, T. Ozawa, Y. Nagata, and H. Samata: J. Alloys Compd. **368** (2004) 51.
27) N. Kase, T. Muranaka, and J. Akimitsu: J. Phys. Soc. Jpn. **77** (2008) 54714.
28) G. E. Volovik: JETP Lett. **58** (1993) 457.
29) E. Helfand and N. R. Werthamer: Phys. Rev. **147** (1966) 288.
30) K. Maki: Phys. Rev. **148** (1966) 362.
31) L. Coffey, K. A. Muttalib, and K. Levin: Phys. Rev. Lett. **52** (1984) 783; L. Coffey, K. Levin, and K. A. Muttalib: Phys. Rev. B **32** (1985) 4382.
32) T. Kita and M. Arai: Phys. Rev. B **70** (2004) 224522.
33) F. Marsiglio and J. P. Carbotte: Phys. Rev. B **41** (1990) 8765.
34) L. N. Bulaevskii, O. V. Dolgov, and M. O. Ptitsyn: Phys. Rev. B **38** (1988) 11290.
35) S. Kuroiwa, Y. Tomita, A. Sugimoto, T. Ekino, and J. Akimitsu: J. Phys. Soc. Jpn. **76** (2007) 094705.
36) K.-W. Lee and W. E. Pickett: Phys. Rev. B **72** (2005) 174505.

Note added in proof—After our paper was submitted, Fang *et al.* have reported about superconducting and normal state of the polycrystalline sample of Ru_7B_3 [arXiv:0811.2252v1].